A survey of Ce^{3+} activated yttrium aluminum garnet phosphors

Bao-gai Zhai[1], Lan-li Chen[2], Ming Yu Li[1], Yuan Ming Huang*

[1] School of Mathematics and Physics, Changzhou University, Jiangsu 213164, China
[2] School of Electronic and Electrical Engineering, Nanyang Institute of Technology, Nanyang, Henan 473007, China
(*Received 15 January 2017; accepted 27 February 2017*)

A survey of Ce^{3+} activated yttrium aluminum garnet phosphors (YAG) is presented. This review includes the historical development, crystal structure, electronic structure, optical properties and a variety of preparation techniques of YAG. The challenges faced by the yellow phosphor are outlined, and the strategies for future improvement are given.

Keywords: YAG; Phosphors; Crystal structure; Electronic structure; Morphology; Photoluminescence

Table of contents

1. Introduction

Yttrium aluminum garnets, $Y_3Al_{55}O_{12}$ (YAG), carry many important technological uses as scintillators [1], magnetic materials, popular laser host materials [2], phosphor materials employed in television screens [3], computer memories and in many devices as microwave optical elements. It is well known that YAG is a material that can be doped with rare earth ions in substitution for Y. Among the doped YAG materials, Ce^{3+} doped YAG nanoparticles are the subject of intensive research motivated essentially by their use in white light emitting diodes (LEDs) [4]. In such an application, the blue emission of a high brightness GaN or InGaN LED is partially absorbed by the Ce^{3+} ions in the YAG nanoparticles and then converted by a photoluminescence (PL) process into yellow light (peaked at 550 nm approximately). In spite of the long history and a wide variety of applications, there is a renewed interest in Ce^{3+} doped YAG due to its application in white LEDs.

In spite of the success of YAG:Ce^{+}, the rapidly expanding market for solid-state lighting has an urgent need for new phosphors with a higher conversion efficiency, a better coverage of the spectrum (including the orange/red spectral region), and an improved thermal quenching behavior. This becomes even more evident when one takes the fast development in the market of high-power LEDs into account. Further, the garnet structure provides a good model for crystal chemical studies by substituting ions in the four, six and eight-fold coordinated positions. In order to provide a pertinent account that will lead to performance increases in the future, here we give a review on the historical development, crystal structures, electronic structures, optical properties and preparation techniques of Ce^{3+} doped YAG. The challenges faced by Ce^{3+} doped YAG are also summarized in this review.

*Corresponding author. Email: dongshanisland@126.com

2. Historical development of YAG

2.1 YAG in ancient times

The story of the garnet dates back to ancient times due to their beautiful colors and hardness. Garnets are a group of silicate minerals that have been used since the Bronze Age as gemstones and abrasives. Garnets, both natural and synthetic, form in a wide range of groups which are closely related by their structure, chemistry, and physical properties. All species of garnets possess similar physical properties and crystal forms, but differ in chemical composition. Garnets are nesosilicates (i,e, orthosilicates, SiO_4) having the general formula $X_3Y_2(SiO_4)_3$. The X site is usually occupied by divalent cations (Ca, Mg, Fe, $Mn)^{2+}$ and the Y site by trivalent cations (Al, Fe, $Cr)^{3+}$ in an octahedral/tetrahedral framework with $[SiO_4]_4$ occupying the tetrahedra. Garnets are most often found in the dodecahedral crystal habit, but are also commonly found in the trapezohedron habit. They crystallize in the cubic system, having three axes that are all of equal length and perpendicular to each other. Garnets do not show cleavage, so when they fracture under stress, sharp irregular pieces are formed.

2.2 YAG in modern era

The scientific history starts in 1928 when Menzer assigned the garnet structure to the space group Ia3d [5]. In 1967, Blasse and Bril were the first to report on Ce^{3+}-doped YAG as a new phosphor for flying-spot cathode ray tubes [6]. The combination of a high luminescence efficiency, a short luminescence lifetime

and a relatively long wavelength (visible) emission made this material ideally suited for this application. The fast emission was shown to be most efficiently excited in the blue (at 460 nm) but it was not until later that this feature was exploited. A good estimate of the luminescence decay time was given (0.07-0.08 μs) [3]. The use of the long wavelength excitation band centered around 460 nm was reported in 1980 [7]. They described the application of YAG:Ce^{3+} in low-pressure mercury vapor discharge lamps to absorb the Hg-plasma lines in the blue/violet part of the spectrum, viz. 405 and 436 nm. The conversion of the violet and blue emission lines into yellow light adds to the white light emitted by the halophosphate phosphor (the commonly used phosphor in those days) to create a warmer white light. It is interesting to note that in the late 1970s some excellent papers were published by Robbins *et al.* on the fundamental aspects of the luminescence and luminescence quenching for Ce^{3+} in YAG [8-10].

2.3 YAG in current days

In the 1990s YAG:Ce^{3+} gained intensive investigations since YAG:Ce^{3+} was proposed as yellow light emitting phosphor to fabricate white LEDs. White LEDs, the so-called next generation solid-state lighting sources, are gaining lots of attentions because of their numerous advantages over the existing incandescent and fluorescent lamps in energy saving, reliability, lifetime and environment-amity. Although the white radiation can be generated from many methods, the combination of a GaN-based blue LED and a YAG:Ce^{3+} phosphor is the most popular and sophisticated method at present [11-16]. For example, Mueller-Mach *et al.* demonstrated a highly efficient warm-white all-nitride phosphor-converted light emitting diode (LED) utilizing a GaN based quantum well blue LED and two novel nitrogen containing luminescent materials, both of which are doped with Eu^{2+} [11]. The fundamental properties of YAG:Ce^{3+} phosphors are investigated [17-20].

3. Fundamental properties of YAG

3.1. Crystal structures of YAG

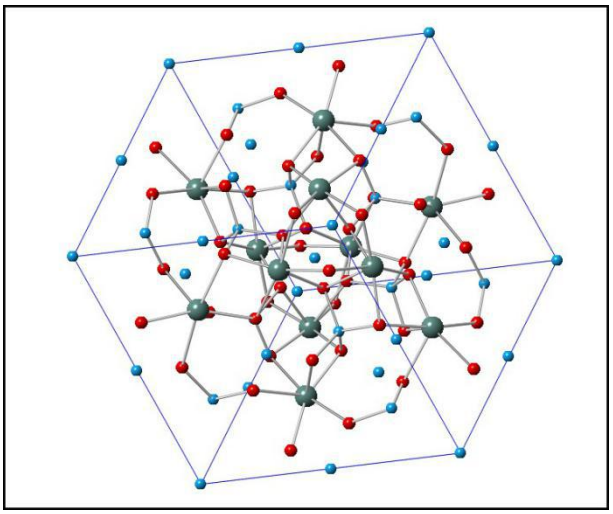

Fig. 1 Stick and ball representation of the primitive unit cell of YAG. The red ball denotes O atom, the sky blue ball represents Al atom while the juniper green ball represents the Y atom.

The YAG system crystallizes in the cubic garnet structure with space group Ia3d (230). In the garnet, there are eight molecules per unit cell but four molecules per primitive cell. Fig. 1 represents the stick and ball representation of the primitive unit cell of YAG. The red ball denotes O atom, the sky blue ball represents Al atom while the juniper green ball represents the Y atom. Since the primitive cell contains four molecules, there are 12 Y sites, 20 Al sites and 48 O sites in the primitive unit cell, making the total number of atoms in the primitive unit cell up to 80.

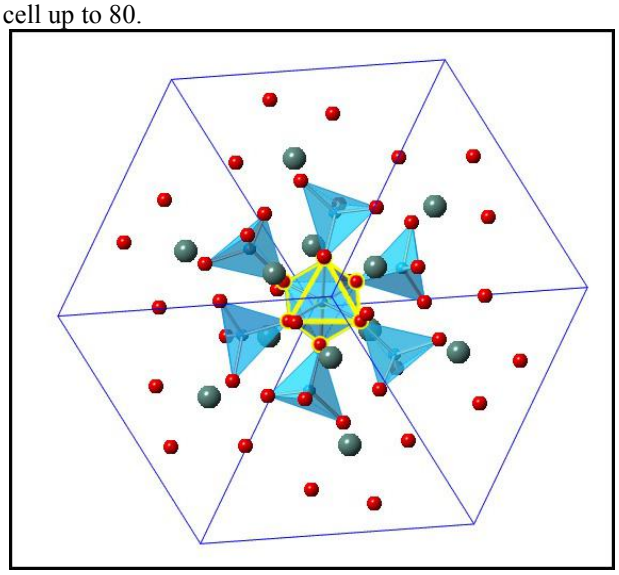

Fig. 2 Schematic illustration of one Al octahedron and six Al tetrahedrons in the primitive unit cell of YAG. The red ball denotes O atom, the sky blue ball represents Al atom while the juniper green ball represents the Y atom.

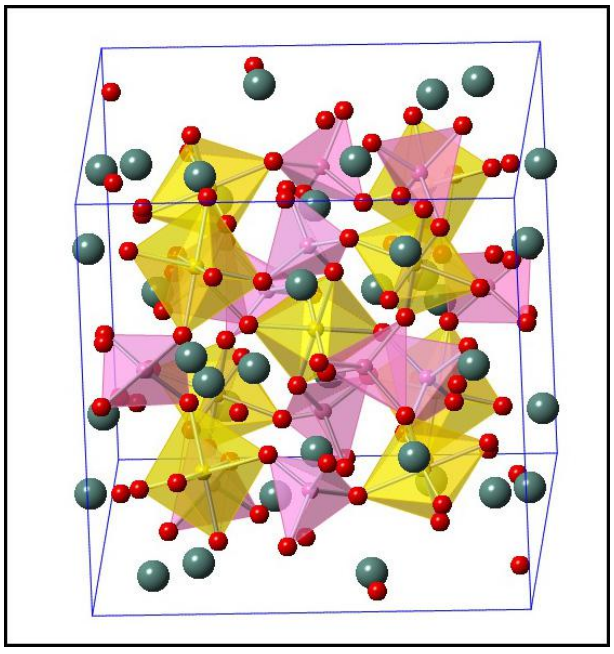

Fig. 3 Stick and ball representation of the conventional unit cell of YAG. The red ball denotes O atom, the sky blue ball represents Al atom while the juniper green ball represents the Y atom.

In this structure, there are two types of Al atoms, of

which two Al atoms are octahedrally and three Al atoms are tetrahedrally coordinated with the O atoms. Fig. 2 schematically illustrates one Al octahedron and six Al tetrahedrons in the primitive unit cell of YAG. Our essential idea of this illustration is to understand the role of 4 and 6 coordinations of Al atoms in YAG. That is, the Al atoms in YAG are either in the 4-fold coordination positions or in 6-fold coordination positions.

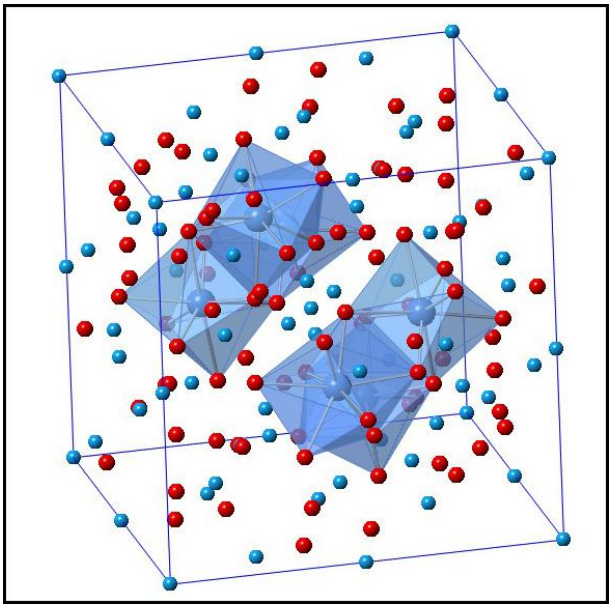

Fig. 4 Stick and ball representation of Y dodecahedrons in the conventional unit cell. The red ball denotes O atom, the sky blue ball represents Al atom while the juniper green ball represents the Y atom.

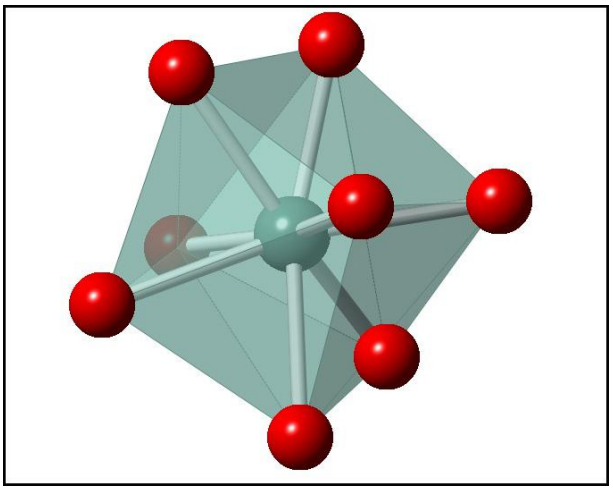

Fig. 5 Stick and ball representation of one Y dodecahedron in the conventional unit cell. Eight oxygen atoms in a distorted dodecahedron coordinate the Y atom, giving it D_2 symmetry.

In the garnet, there are eight molecules per conventional unit cell. So the conventional unit cell contains 24 Y sites, 40 Al sites and 96 O sites, making the total number of atoms up to 160 in the unit cell. Fig. 3 shows the stick and ball representation of the conventional unit cell of YAG. The red ball denotes O atom, the sky blue ball represents Al atom while the juniper green ball represents the Y atom. The tetrahedrons (pink) and octahedrons (yellow) can be clearly distinguished. In the structure of YAG, the Y atoms are dodecahedrally coordinated. Fig. 4 illustrates the stick and ball representation of six Y dodecahedrons in the conventional unit cell. The red ball denotes O atom, the sky blue ball represents Al atom while the juniper green ball represents the Y atom. Eight oxygen atoms in a distorted dodecahedron coordinate the Y atom, giving it D2 symmetry. These dodecahedrons are connected with each other by sharing edges.

In order to illustrate the coordination of Y to O atoms, we show solely one Y dodecahedron in the conventional unit cell of YAG. Fig. 5 represents the stick and ball representation of one Y dodecahedron in the conventional unit cell. It is obvious that one Y atom is coordinated with 8 O atoms.

3.2 Electronic structures of YAG

The band structure of a given semiconductor is pivotal in determining its potential utility. Consequently, an accurate knowledge of the band structure is critical if the semiconductor in question is to be incorporated in the family of materials considered for device applications. Thus, the electronic structure of Ce^{3+} doped YAG is the most important factor to determine the optical properties of the phosphor. Several theoretical approaches of varying degrees of complexity were employed to calculate the band structure of YAG [21-23].

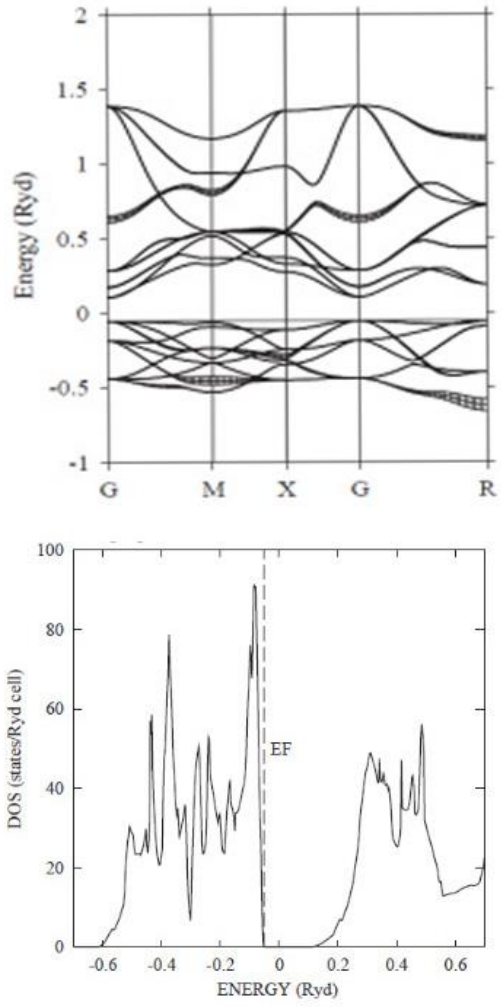

Fig. 6 Band structures of YAG and TDOS of undoped YAG.

For the pure and doped garnet systems, there are very few theoretical electronic structure studies in the literature. To our knowledge, no ab initio or first principles electronic structure calculations of important garnets are available except the works of D'Arco *et al.* [21] for $Mg_3Al_2Si_3O_{12}$ and Pari *et al.* [22], and Xu *et al.*[23] for YAG. The reason perhaps is the difficulty of dealing with the rather large unit cell. For example, D'Arco *et al.* calculated the electronic structures of $Mg_3Al_2Si_3O_{12}$, the total and projected density of states indicated that pyrope is a highly ionic insulator with a large band gap of about 17 eV [21]. In order to study quantitatively and systematically the electronic structural properties of the $R_3Al_{55}O_{12}$ with R = Ce-Lu, where the R atoms are substituted at the dodecahedrally coordinated Y sites in YAG, Pari *et al.* performed first-principles electronic structure calculations of $R_3Al_{55}O_{12}$ (R = Ce – Lu), using the tight-binding linearized muffin-tin orbital method within local density approximation [22]. Fig. 6 shows the calculated band structures and total density of states (TDOS) of undoped YAG. The fat bands in Fig. 6 indicate the characters of a band. The fatness of the bands allows us to determine which electronic states give rise to which bands. The band gap value of undoped YAG is about 0.2 Ryd, which is equal to 2.72 eV. However, there are no experimental results available to compare with the calculated results. It is important to note that the insulating gap of 3.75 eV for $Lu_3Al_{55}O_{12}$ (is direct at G point) occurs between the O-2p and the empty R-5d.

Ning *et al.* investigated geometric and electronic structures of Ce^{3+} and Si – N co-doped YAG with first principles methods to gain microscopic insight into effects of Si – N addition on electronic structures and optical properties of Ce^{3+} [24]. Hybrid density functional theory (DFT) calculations reveal that the Si–N prefers to be substituted for the tetrahedral Al(tet) – O sites with a random distribution. Fig. 7 shows the total and orbital-projected DOSs for the YAG unit cell calculated by DFT with the PBE0 hybrid functional containing 32% HF exchange and a $2\times2\times2$ k-point grid to sample the Brillouin zone. Moreover, from the values of $\varepsilon(Ce^{3+/4+})$ and the band gap (E_g = 7.68 eV) of the host, the energy difference between the Ce^{3+} $4f^1$ ground-state level and the host conduction band maximum is 3.85 eV, which is in good agreement with that (3.8 eV) as estimated from photoconductivity measurements on YAG:Ce^{3+}.

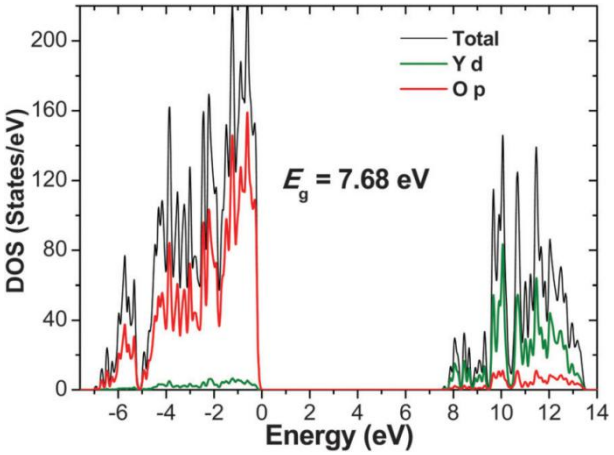

Fig. 7 Total and orbital-projected DOSs for the YAG unit cell calculated by DFT with the PBE0 hybrid functional containing 32% HF exchange and a 2×2×2 k-point grid to sample the Brillouin zone. The Fermi level is set at zero energy.

3.3 Optical properties of YAG:Ce^{3+}

The optical properties are the core of Ce^{3+} doped YAG for the desired application. Among the a variety of optical properties, the PL and excitation spectra are the most important ones [17-20].

3.3.1 Concentration dependent PL

It is naturally expected that the concentration of Ce3+ dopant generates significant effects on the optical properties of the yellow phosphor. Masenelli *et al.* investigated the luminescence properties of 10 nm YAG nanoparticles doped with Ce^{3+} ions at 0.2%, 4% and 13% that are designed as active probes for scanning near-field optical microscopy [14]. Fig. 8 shows the 5d → 4f Ce^{3+} emission transitions probed by PL of the YAG nanoparticles doped with Ce^{3+} at 0.2%, 4% and 13% from top to bottom, respectively. The nanoparticles were produced by a physical method without any subsequent treatment, which is imposed by the desired application. The emission of the 13% doped Ce:YAG nanoparticles is marginal and not representative of the samples, in which most parts do not emit light. The relative intensities are arbitrary and have been set only for the sake of clarity. In contrast to the 0.2% and 4% doped nanoparticles, which were excited at a 450 nm wavelength, the 13% doped nanoparticles were excited at a 220 nm wavelength [14]. The structural analysis reveals the amorphous nature of the particles, which we relate to some compositional defects as indicated by the elemental analysis. The optimum emission is obtained with a doping level of 4%. The emission of the YAG nanoparticles doped at 0.2% is strongly perturbed by the crystalline disorder whereas the 13% doped particles hardly exhibit any luminescence. In the latter case, the presence of Ce^{4+} ions is confirmed, indicating that the Ce^{3+} concentration is too high to be incorporated efficiently in YAG nanoparticles in the trivalent state.

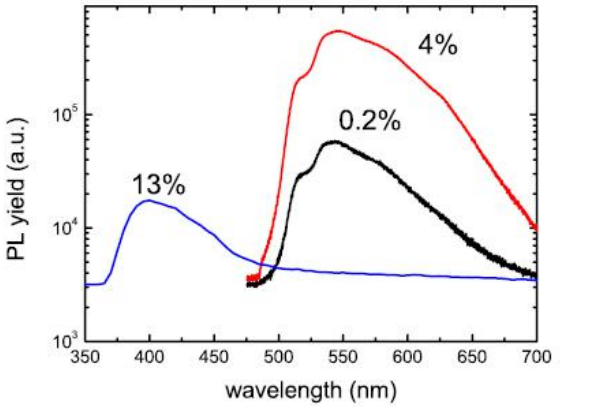

Fig. 8 5d → 4f Ce^{3+} emission transitions probed by PL of the YAG nanoparticles doped with Ce^{3+} at 0.2%, 4% and 13% from top to bottom, respectively [14].

Fig. 9 represents the PL decay curves of the Ce:YAG nanoparticles doped at 0.2% and 4%. The triangle and square symbols are fits to the decay curves of the 0.2%

and 4% doped nanoparticles, respectively. Time-resolved PL reveals the presence of quenching centers likely related to the crystalline disorder as well as the presence of two distinct Ce^{3+} ion populations. Eventually, nano-cathodoluminescence indicates that the emission and therefore the distribution of the doping Ce^{3+} ions and of the defects are homogeneous [14].

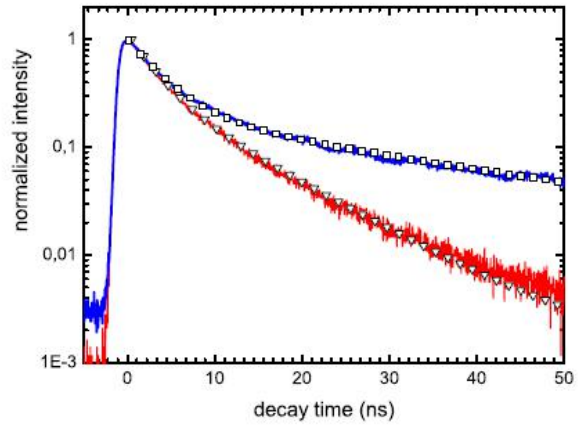

Fig. 9 PL decay curves of the Ce:YAG nanoparticles doped at 0.2% and 4%. The triangle and square symbols are fits to the decay curves of the 0.2% and 4% doped nanoparticles, respectively.

3.3.2 Calcination temperature dependent PL

It is well known that annealing can significantly changes the optical properties of a luminescent material. Yuan and Ryu reported the PL of Ce-doped YAG phosphor powders prepared by co-precipitation [25]. Ce-doped YAG phosphor powders were prepared by co-precipitation methods using ammonium hydrogen carbonate as precipitant. Pure Ce-doped YAG phase was obtained by calcining the precipitate at 1200 °C. The emission intensity of Ce-doped YAG phosphor was found to increase with the increases in the calcining temperature, and there was a clear shift of peaks to longer wavelengths. Fig. 10 shows the XRD patterns of as-calcined Ce-doped YAG powders

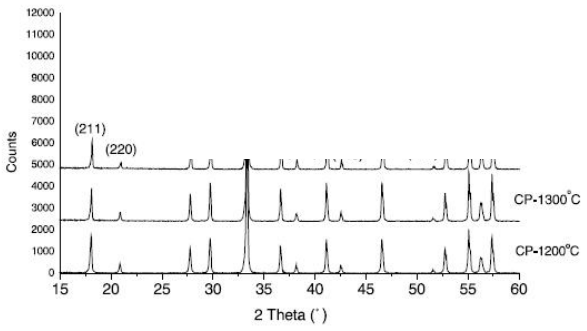

Fig. 10 XRD patterns of as-calcined Ce-doped YAG powders.

at different temperatures. The XRD patterns indicate YAG to be the only crystalline component at calcining temperature over 1200 °C. There are three stable phases in the Y_2O_3 – Al_2O_3 binary systems: YAG, $YAlO_3$ (perovskite) and $Y_4Al_2O_9$ (monoclinic structure). It is reported that YAG phase can be obtained at higher temperature over 1600 °C in the conventional solid-state reaction for $Y_2O_3-Al_2O_3$ binary systems. However, pure YAG phase is produced for samples prepared by precipitation methods at a calcining temperature at 1200 °C, which is near 400 °C lower than conventional solid-state method. As the XRD pattern shows, moreover, further calcining at higher temperatures leads to the increases in the YAG diffraction peak intensity and reduces in the full-width at half-maximum due to the improvement of crystallinity and growth.

Fig. 11 shows the emission spectra of Ce-doped YAG prepared by co-precipitation. It can be seen that emission intensity increases with the increase in calcining temperature for both samples. The emission of Ce^{3+} occurs from the lowest crystal field component of $5d^1$ configuration to the two levels of the ground state $^2F_{5/2}$ and $^2F_{7/2}$, which is separated by some 2000 cm^{-1} due to spin–orbit coupling. The shift of peaks to longer wavelength indicates that the lowest 5d has a shift to higher energy level. The shift of peaks in Ce-doped YAG phosphor has also been found in the samples prepared by citrate gel and polyacrylamide methods. It is reported that the change of unit cell affect the crystal field around Ce^{3+}, and causes the blue-shift phenomena of spectra. As the XRD data indicate, the 2θ value has a little increase with calcining temperature increase, as a result, the lattice parameter decrease as well, thereby, it is reasonable that the change of crystal field induces the shift of peaks.

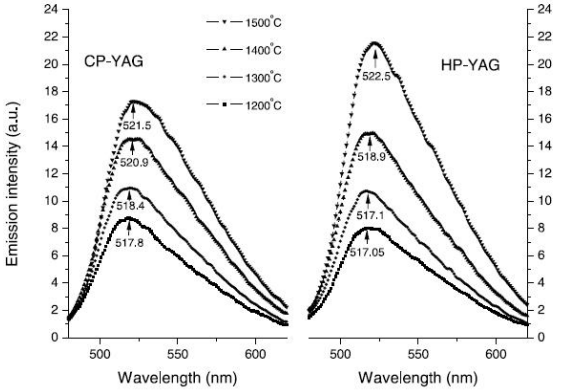

Fig. 11 Emission spectra of Ce-doped YAG prepared by co-precipitation.

3.3.3 Temperature dependent PL

The temperature of the phosphor is another parameter to influence its optical properties. The work of Robbins was focused on the behavior between 4 and 400 K [9]. The variation of the light output was shown to be complex and to involve changes in the absorption strength of the (different) f-d absorption bands and the (temperature-dependent) energy transfer to defects. After this work, research on the fundamental understanding of the temperature quenching of the luminescence in YAG:Ce^{3+} is limited. Recently, Shao *et al.* published one piece of paper on this subject. Fig. 12 shows the relative luminance of the pure and Gd^{3+} doped YAG phosphor at varying temperature (25 – 200 °C) [26]. Gd^{3+}-doped, La^{3+}-doped and Gd^{3+}/La^{3+} co-doped YAG:Ce^{3+} phosphors were prepared by high-temperature solid-state reaction. Their crystal structure and PL properties at various

temperatures (25 – 200 °C) were investigated. The luminance of the samples at elevated temperature is normalized to that at 25 °C. The pure YAG:Ce^{3+} exhibits a remarkable thermal quenching behavior. Its luminance falls by 12% at 150 °C, and by 20% at 200 °C. The introduction of Gd^{3+} significantly increases the temperature sensitivity of YAG:Ce^{3+}. The relative luminance of $Y_{0.43}Gd_{2.5}Al_{55}O_{12}$:$Ce_{0.07}$ falls by 70% at 150 °C, and by 87% at 200 °C.

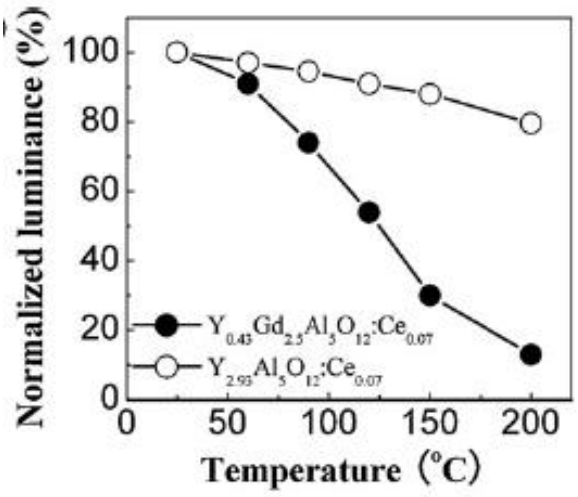

Fig. 12 Normalized luminance of $Y_{2.93}Al_5O_{12}$:$Ce_{0.07}$ and $Y_{0.43}Gd_{2.5}Al_5O_{12}$:$Ce_{0.07}$ phosphors at various temperatures [26].

4. Preparation methods

The preparation method influences the morphology, phase, optical properties and costs of Ce^{3+} doped YAG. Therefore it becomes necessary to know the preparation techniques.

4.1 Solid state reaction method

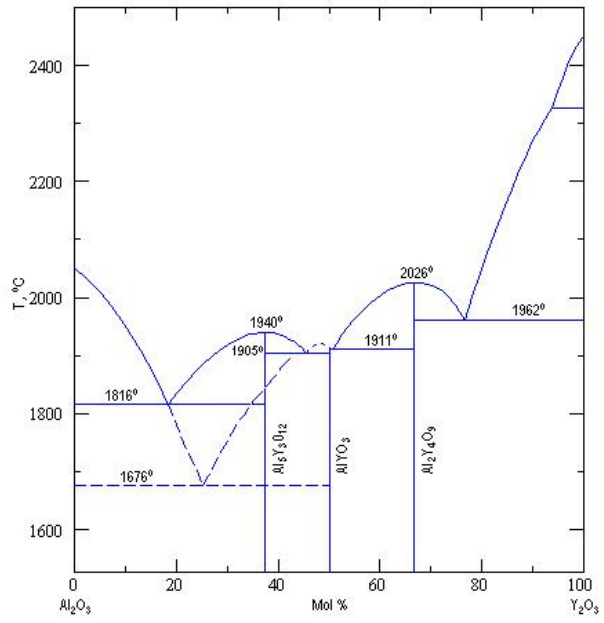

Fig. 13 Phase diagram of Y_2O_3-Al_2O_3 binary system.

YAG powders are conventionally prepared by a solid-state reaction process at a high reaction temperature (>1600 °C). In the solid-state reaction process, agglomerated large particles (5-20 mm) of irregular shapes and several intermediate phases such as $YAlO_3$ and $Y_4Al_2O_9$ are produced. Also, replacing Y^{3+} ions by larger ones in YAG:Ce^{3+} is a tedious process in solid-state reaction method. The synthesis of pure-phase YAG powder by solid-state reaction process is documented in the literature [27-30].

Fig. 13 illustrates the phase diagram of Y_2O_3-Al_2O_3 binary system. The molar ratio of Y_2O_3 in the starting materials (Y_2O_3 and Al_2O_3) must be 0.375 in order to synthesize YAG. It is clear in Fig. 13 that high temperature is required to synthesize YAG. In mass production, solid state reaction method is widely used in the synthesis of YAG:Ce^{3+} phosphors. However, this method has a few inevitable disadvantages: it normally requires high calcination temperature (1500 °C) and long ball-milling time. High temperature leads to the formation of coarse and heavily agglomerated particles, which need further milling process or other procedures to make the phosphor powders suitable for the use in LED packaging. In addition, the extensive ball milling could lead to impurity contamination and degeneration of the luminescence properties of the phosphors.

4.2 Sol-gel method

In the synthesis of powders, hydrothermal method that uses supercritical water as a reaction media exhibits great advantages in synthesizing powders, such as low reaction temperature, no organic contamination and so on. So, by using the hydrothermal and solvothermal methods, these garnet phosphors were obtained at low reaction temperatures without being subject to additional heat treatment [31-33]. The crystallization by this method has faster growth rate compare to solvothermal synthesis. The sol-gel method show advantages of high purity, homogenous composition, fine grains and lower sintering temperatures when compared to the solid-state reaction method [31-33]. These methods require additional heat treatment at higher temperatures (>800 °C) to get well crystallized products. Using water and ethyleneglycol as the solvent, Boukerika *et al.* prepared the precursor for subsequent annealing at 900 °C to synthesize YAG:Ce^{3+} [31]. Katelnikovas *et al.* prepared the precursor for subsequent annealing at 1000 °C to synthesize YAG:Ce^{3+} [32]. With malic acid and polyethylene glycol in water, Sun *et al.* prepared the precursor for subsequent annealing at 900 °C to synthesize YAG:Ce^{3+} [33].

4.3 Solvothermal method

Solvothermal method is another kind of technique to synthesize YAG:Ce^{3+} phosphor [34-38]. Park *et al.* prepared Ce^{3+} doped YAG phosphors via the solvothermal method [34]. The crystalline powders were prepared with stoichiometry amounts of reagents. In a process, all reagents were dissolved in 20 ml of 2-propanol at the concentration of 5 mol%. The mixed solution was vigorously stirred by using magnetic stirrer for 1 h until the homogeneous solution was formed and transferred into a glass vial (40 ml capacity and 50%) and this was placed into a stainless steel autoclave. The mixture was then heated to 300 °C at a rate of 10 °C min^{-1} with magnetic stirring to mix the solutes homogeneously and the temperature was maintained at 300 °C for 48 h without stirring to enable the crystallization of mixed

solution. After 48 h, the autoclave allowed to cool room temperature. The crystalline powders were collected by a centrifugal separator with 4000 rpm for 5 min and then washed with absolute ethanol several times to remove the excess-reactants and by-products. Finally, the product was dried at 60 °C for 5 h in ambient atmosphere.

The top panel in Fig.14 shows the XRD patterns of $Y_3Ga_2Al_3O_{12}$ sample obtained at various reaction temperatures for 48 h [34]. As shown in Fig. 14, it was observed that no diffraction peaks appeared up to 280 °C, which indicate that the sample is in amorphous state at 280 °C and below. When the calcination temperature reached to 300 °C, all the diffraction peaks were quite consistent with the standard data from JCPDS card 89-6685 of $Y_3Ga_2Al_3O_{12}$. The bottom panel in Fig. 14 illustrates the normalized PL spectra of Ce^{3+} doped $Ln_3Al_2Al_3O_{12}$ crystalline powders: (a) $Y_3Al_2Al_3O_{12}$, (b) $Tb_3Al_2Al_3O_{12}$, (c) $Gd_3Al_2Al_3O_{12}$, and (d) $Sm_3Al_2Al_3O_{12}$.

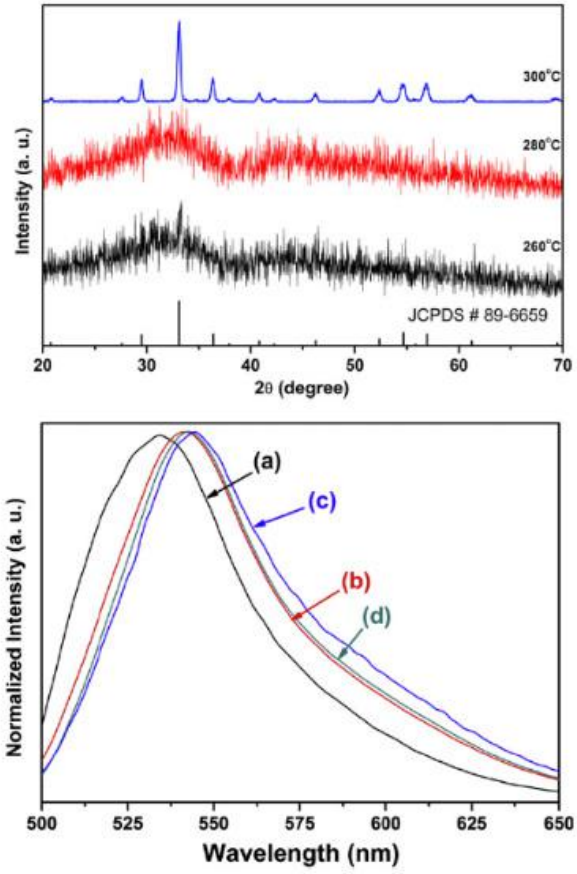

Fig. 14 Top panel: the XRD patterns of $Y_3Ga_2Al_3O_{12}$ sample obtained at various reaction temperatures for 48 h. Bottom panel: the normalized PL spectra of Ce^{3+} doped $Ln_3Al_2Al_3O_{12}$ crystalline powders: (a) $Y_3Al_2Al_3O_{12}$, (b) $Tb_3Al_2Al_3O_{12}$, (c) $Gd_3Al_2Al_3O_{12}$, and (d) $Sm_3Al_2Al_3O_{12}$.

4.3 Co-precipitation method

Co-precipitation process can make the reaction elements mix homogeneously in the precipitation, whereas, heterogeneous precipitation process is almost the same as solid-state process [35]. Generally, co-precipitation is a good process for preparation of homogeneous mixture, which has been widely used in preparation of ultra-fine powders [31-33]. Although heterogeneous precipitation is nearly the same as the solid-state process, it can make a special unit for precipitation precursor, which can make the core Al and shell Y and Ce^{3+} compounds have a shorter distance and a homogeneous unit distribution than that for solid-state sample. Furthermore, the special unit can give some advantages for distribution of doped cerium in the YAG lattices, which can help to increase the emission intensity. It is reported that the reaction between Y_2O_3 and Al_2O_3 occurs by the diffusion of Al into Y_2O_3 in the conventional solid-state synthesis process. The reaction between Y_2O_3 and Al_2O_3 for the powders prepared by heterogeneous precipitation mentioned here is the same as that in solid-state process, except that the reaction for these powders is faster because of fine starting particles. In this process, cerium and yttrium compounds are mixed homogeneous, which can make the doped cerium diffuses into the YAG lattice homogeneous, especially at high temperature.

4.5 Microemulsion method

The synthesis of nanoparticles by microemulsion method has been widely reported in the literature. Microemulsion method can be utilized to synthesize YAG:Ce^{3+} [39]. Spherical nanopowder of YAG:Ce^{3+} was prepared by the microemulsion method in a water / Triton X–100 / hexanol / (cyclohexan+n-hexane) system. Al, Y and Ce chloride and nitrates were used as starting materials, and ammonia was used as a precipitating agent. The procedures of the microemulsion synthisis are outlines as follows: (1) Stoichiometric amounts of yttrium nitrate hexahydrate, aluminum chloride hexahydrate and cerium nitrate hexahydrate, were dissolved in deionized-distilled water in a crucible. The ratios of n(Y)/n(Al)/n(Ce) were set as (3–x)/5/x (x=0.04–0.1) according to $Y_{3-x}Al_5O_{12}:xCe^{3+}$. The concentration of all cations of the aqueous solution was 0.64 mol/L (reactant solution), whereas the ammonia solution was diluted with deionized-distilled water to 2.5 mol/L (precipitant solution). (2) Two water / Triton X–100 / hexanol / (cyclohexan+n-hexane) microemulsions, A and B, differing only in the aqueous phase, were prepared. The aqueous phase of microemulsion A was the reactant solution, whereas the aqueous phase of microemulsion B was the precipitant solution. The composition of the four-component microemulsion is defined by the water/surfactant (Triton X–100) molar ratio, R, and the co surfactant (hexanol)/surfactant molar ratio, P (R=39.9, and P=3.7). (3) Microemulsion B was added dropwise to microemulsion A maintained under constant stirring at room temperature until a pH value of 8 was reached. A white hue sol was instantaneously observed, indicating the formation of hydroxides. (4) Complete precipitation occurred in 12 h. The mixed cerium–yttrium–aluminum hydroxide precipitate was filtered and repeatedly washed with water to remove residual ammonia, chloride ions, nitrate ions, and surfactant molecules. (5) Finally the precipitate was washed with ethanol to facilitate the drying process. The obtained white precipitate was oven dried at 60 °C, the residual carbon was eliminated and the sample was calcined at 700–900 °C for 2 h under mild

reducing atmosphere [39].

The YAG:Ce^{3+} nanopowder was prepared successfully. The top panel in Fig. 15 shows the XRD patterns of as-prepared powders after carbon removal calcined at various temperatures for 2 h. The bottom panel in Fig. 15 depicts the TEM micrograph of the YAG:Ce^{3+} phosphor powders. Experimental results indicate that the pure YAG phase is synthesized at the temperature of 800 °C, which is lower than that by solid-state method (over 1500 °C). The results show that the YAG:Ce^{3+} nanopowder consist of fairly uniform, spherical particles. The particle size is distributed uniformly at 50 nm. The excitation spectra show two peaks, with the major one at 469 nm. The emission spectra peak is at 532 nm, indicating that phosphor is qualified for use in white light emitting diode.

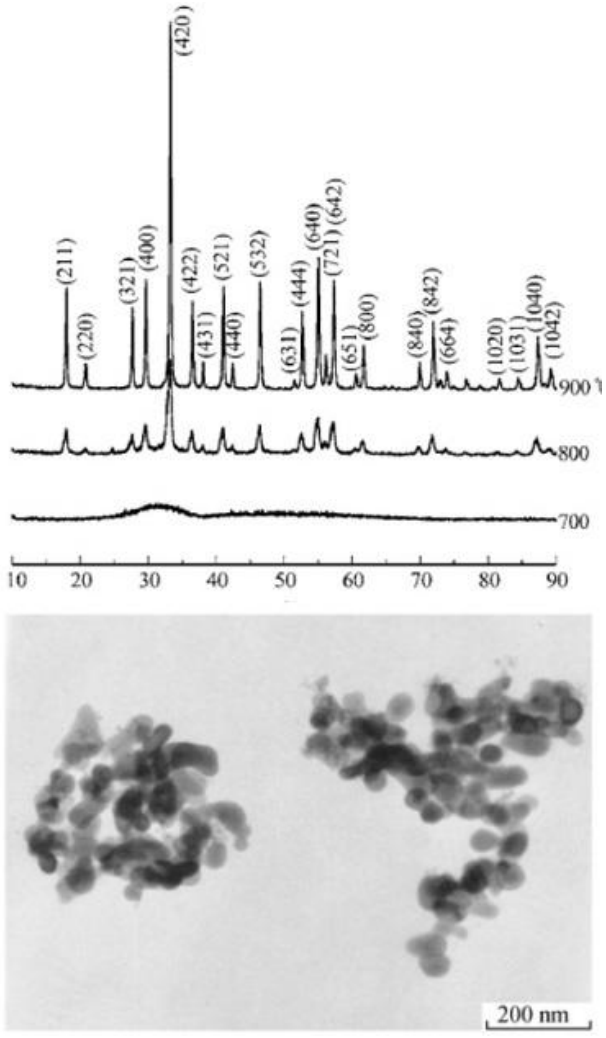

Fig. 15 Top panel: XRD patterns of as-prepared powders after carbon removal calcined at various temperatures for 2 h. Bottom panel: TEM micrograph of the YAG:Ce^{3+} phosphor powders.

4.6 Combustion method

Mukherjee *et al.* Prepared lanthanide ions (Ce^{3+}, Eu^{3+}, Dy^{3+} and Tb^{3+}) doped YAG by glycine nitrate combustion method followed by annealing at a relatively low temperature of 800 °C [40]. For the preparation of undoped and Eu^{3+} doped YAG nanoparticles, stoichiometric amounts of solid oxides of yttrium and europium along with $Al(NO_3)_3 \cdot 9H_2O$ were dissolved in aqueous nitric acid. Required amount of glycine was added by keeping the nitrate to glycine ratio 1.2. The solution was slowly heated at 100 °C on a hot plate to get a colourless gel. Temperature was then raised to 200 °C so that combustion reaction took place to form a white fluffy powder. The powder was initially heated to 600 °C followed by heating to 800 and 1200 °C for 4 h each. Their XRD pattern shows the product obtained after combustion reaction followed by heat treatment at 600 and 800 °C. Samples annealed at 600 °C are found to be amorphous. However on heating to 800 °C, crystalline nanoparticles with YAG structure are formed. Naik *et al.* Cr and Nd co-doped Ce:YAG compounds via the sol–gel autocombustion technique. A reduction in the formation temperature to 1000 °C is required [41].

4.7 Other methods

Other methods were also employed to synthesize Ce^{3+} doped YAG. Examples include the microwave method [42], micro-pulling down technique [43,44], electrospinning method [45], Czochralski (CZ) method [46], molten salt method [47].

5 Challenges and strategies

White LEDs become the next generation solid-state lighting sources. YAG doped with Ce^{3+} is known as an efficient yellow phosphor with high internal luminescence quantum yield (>90%) and perfect photostability. One of its broad absorption bands peaks at 450 nm and matches perfectly the blue-emitting LEDs for the generation of white light [26,48]. However, this strategy suffers from low color-rendering index (CRI) and high color-temperature due to the weak emission intensity in red spectral region [48].

The first challenge is that the emission wavelength lacks a red component, producing a so-called " cold " white light. A color rendering index (CRI) is a quantitative measure of the ability of a light source to reveal the colors of various objects faithfully in comparison with an ideal or natural light source. Light sources with a high CRI are desirable in color-critical applications such as neonatal care and art restoration. The CRI of a light source does not indicate the apparent color of the light source. The CRI is determined by the light source's spectrum. Numerically, the highest possible CIE Ra value is 100, and would only be given to a source identical to standardized daylight or a black body (incandescent lamps are effectively black bodies), dropping to negative values for some light sources. Using a large rare earth ion, such as $Gd^{3+}$and Tb^{3+}, to substitute the dodecahedral site of the garnet structure can shift the Ce^{3+} emission band to a longer wavelength because of the larger crystal splitting of the 5d energy level of Ce^{3+} ions. It is beneficial to improve the color-temperature and color-rendering properties of w-LEDs based on YAG:Ce^{3+} phosphor [49].

The second challenge is that the quantity of Ce^{3+} ions that can be incorporated into the YAG matrix is small due to the mismatch between the Ce^{3+} ionic radius (1.143 Å for a coordination number of 8) and the substituted Y^{3+} ionic radius (1.019 Å for a coordination number of 8). The maximum concentration is reported as 3 at.% when

YAG:Ce^{3+} is synthesized by solid state reaction. This results in a small absorption of the blue light of the GaN diode, and a large amount of powder or ceramics is required to acquire the appropriate yellow component from the device. Additional drawbacks include re-absorption and strong scattering that reduces the external quantum efficiency of these white LED devices.

The third challenge is that the synthetic temperature of Ce^{3+} activated YAG is as high as 900 ºC. Although about a dozen of techniques are employed to synthesize Ce^{3+} doped YAG, a subsequent calcination is often necessary to turn the precursor into YAG. It would be beneficial if we can lower the synthesis temperature to 300 ºC.

The fourth challenge is that the fundamental aspects of Ce^{3+} doped YAG are still not well understood. Example include the accurately determined bandgap values of YAG, the accurate calculation of the electronic structure of Ce^{3+} doped YAG, and the depths of a variety of defect energy levels in YAG. On one hand, some workers calculated the band structures of YAG, but those results are hard to compare to experimental observation [21-24,50]. As documented in the literature, several groups explored the roles of intrinsic and extrinsic defects in YAG [51-53]. In spite of these research activities, the understanding of the roles of defects is limited. It is obvious that thorough investigations on these fundamental issues can provide insight into the optical properties for Ce^{3+} in YAG.

The strategies to facing these chanllenges rest on the wisdom and hard work of mankind. For example, in order to increase the CRI of Ce^{3+} doped YAG, it is interesting to note that some authors have turned to alternative host materials [54-57]. For example, Krevel *et al.* observed blue-green emission from Ce^{3+} activated Y-Si-O-N materials [54]; Li *et al.* reported red emissions from Eu^{2+} activated $M_2Si_5N_8$ (M = Ca, Sr, Ba) LED conversion phosphors [55]; Lee *et al.* reported a novel reddish orange-emitting $BaLa_2Si_2S_8$:Eu^{2+} thiosilicate phosphor for LED lighting [56]. Another example is that the state-of-the-art DFT calculations may provide the most accurate information on the band structures, bandgap values and defect energy levels in YAG, as they did in other ceramics such as ZnO [58], $SrAl_2O_4$ [59] and ZnMoO4 [60].

4. Conclusions

It is the aim of this paper to provide a survey of Ce^{3+} activated YAG:Ce^{3+} nanoparticles, which is especially relevant for new comers to white LEDs. A survey of the well-established and newly emerging yellow phosphor Ce^{3+} activated YAG is presented. The review includes the historical development, the crystal structure, the electronic structure, optical properties and preparation techniques of YAG. Moreover, the challenges to the yellow phosphor are outlined, and strategies for improvement are given.

Acknowledgment

This work was financially supported by Natural Science Foundation of China under the Grant No 11574036.

References

[1] C.L. Wang, D. Solodovnikov, K.G. Lynn. Point defects in Ce-doped $Y_3Al_5O_{12}$ crystal scintillators. *Phys. Rev. B* 73 (2006) 233204.

[2] J.E. Geusic, H.M. Marcos, L.G. Van Uitert. Laser oscillations in Nd-doped yttrium aluminum, yttrium gallium and gadolinium garnets. *Appl. Phys. Lett.* 4 (1964) 182–184.

[3] G. Blasse, A. Bril. A new phosphor for flying spot cathode–ray tubes for color television: yellow emitting $Y_3Al_5O_{12}$:Ce^{3+}. *Appl. Phys. Lett.* 11 (1967) 53–55.

[4] V. Bachmann, C. Ronda, A. Meijerink. Temperature quenching of yellow Ce^{3+} luminescence in YAG:Ce. *Chem. Mater.* 21 (2009) 2077–2084.

[5] G.Z. Menzer. Die Kristallstruktur der Granate. *Z. Kristallogr.* 69 (1928) 300–396 (in German).

[6] G. Blasse, A. Bril. Investigation of some Ce^{3+}–activated phosphors. *J. Chem. Phys.* 47 (1967) 5139–5145.

[7] E.F. Wyner, A. Daigneault. Improved mercury lamp for low color temperature applications. *J. Illum. Eng. Soc.* 9 (1980) 109–114.

[8] D.J. Robbins, B. Cockayne, J.L. Glasper, B. Lent. Temperature-dependence of rare-earth activated garnet ohosphors.1. Intensity and lifetime measurements on undoped and Ce-doped $Y_3Al_5O_{12}$. *J. Electrochem. Soc.* 126 (1979) 1213–1220.

[9] D.J. Robbins, B. Cockayne, J.L. Glasper, B. Lent. Temperature-dependence of rare-earth activated garnet ohosphors. 2. Comparative-study of Ce^{3+}, Eu^{3+}, Tb^{3+}, and Gd^{3+} in $Y_3Al_5O_{12}$. *J. Electrochem. Soc.* 126 (1979) 1221-1228.

[10] D.J. Robbins. Effects of crystal-field and temperature on the photo-luminescence excitation efficiency of Ce^{3+} in YAG. *J. Electrochem. Soc.* 126 (1979) 1550–1555.

[11] R. Mueller-Mach, G. Mueller, M.R. Krames, H.A. Hoppe, F. Stadler, W. Schnick, T. Juestel, P. Schmidt. Highly efficient all-nitride phosphor-converted white light emitting diode. *Phys. Status Solidi A* 202 (2005) 1727–1732.

[12] T. Tamura, T. Setomoto, T. Taguchi. Illumination characteristics of lighting array using 10 candela-class white LEDs under AC 100 V operation. *J. Lumin.* 87-89 (2000) 1180.

[13] M.R. Krames, O.B. Shchekin, R. Mueller-Mach, G.O. Mueller, L. Zhou, G. Harbers, M.G. Craford, Status and future of high-power light-emitting diodes for solid-state lighting. *J. Display Techn.* 3 (2007) 160–175.

[14] B. Masenelli, O. Mollet, O. Boisron, B. Canut, G. Ledoux, J.-M. Bluet, P. Melinon, Ch. Dujardin, S. Huant. YAG:Ce nanoparticle lightsources. *Nanotechnology* 24 (2013) 165703.

[15] A.A. Setlur, W.J. Heward, Y. Gao, A.M. Srivastava, R.G. Chandran, A.V. Shankar. Crystal chemistry and luminescence of Ce^{3+}-doped $Lu_2CaMg_2(Si,Ge)_3O_{12}$ and its use in LED based lighting. *Chem. Mater.* 18 (2006) 3314–3322.

[16] A.A. Setlur, A.M. Srivastava. The nature of Bi^{3+} luminescence in garnet hosts. *Opt. Mater.* 29 (2006) 410–415.

[17] M. Vorsthove, U. Kynast. Efficiency issues in Ce^{3+} doped YAG nanocrystals. *Mater. Res. Bull.* 46 (2011) 1761–1765.

[18] M.A. Shvaleva, L. A. Nikulina, V. A. Aseev, K.D. Mynbaev, V. E. Bougrov, A.R. Kovsh, M.A. Odnoblyudov, N.V. Nikonorov, A.E. Romanov. Ce^{3+}:YAG doped glass-ceramics for white light-emitting diode. *Opt. Rev.* 21 (2014) 683–686.

[19] Y. Zhao, H. Xu, X. Zhang, G. Zhu, D. Yan, Q. Ling, M. Chen, A. Yu. Optical performances of YAG:Re^{3+} (Re = Ce, Eu) phosphor

films with co-doping Tb^{3+} as energy-transfer sensitizer. *J. Am. Ceram. Soc.* 99 (2016) 756–759.

[20] S. Mukherjee, V. Sudarsan, R.K. Vatsa, A.K.Tyagi. Luminescence studies on lanthanide ions (Eu^{3+}, Dy^{3+} and Tb^{3+}) doped YAG:Ce nano-phosphors. *J. Lumin.* 129 (2009) 69–72.

[21] Ph. D ' Arcoy, F.F. Favaz, R. Dovesiz, V. R. Saunders. Structural and electronic properties of pyrope garnet ($Mg_3Al_2Si_3O_{12}$): an ab initio study. *J. Phys.: Condens. Matter* 8 (1996) 8815–8828.

[22] G. Pari, A. Mookerjee,, A.K. Bhattacharya, First-principles electronic structure calculations of $R_3Al_5O_{12}$ (R being the rare-earth elements Ce–Lu), *Physica B* 365 (2005) 163–172.

[23] Y.N. Xu, W. Y. Ching. Electronic structure of yttrium aluminum garnet. $Y_3Al_5O_{12}$. *Phys. Rev. B* 59 (1999) 10530–10535.

[24] L. Ning, X. Ji, Y. Dong, W. Jin, Y. Huang, Z. Pan, P. A. Tanner, First-principles study of Ce-doped $Y_3Al_5O_{12}$ with Si – N incorporation: electronic structures and optical properties, *J. Mater. Chem. C* 4 (2016) 5214–5221.

[25] F. Yuan, H. Ryu. Ce-doped YAG phosphor powders prepared by co-precipitation and heterogeneous precipitation. *Mater. Sci. Eng. B*107 (2004) 14–18.

[26] Q. Shao, H. Li, Y. Dong, J. Jiang, C. Liang, J. He, Temperature-dependent photoluminescence studies on $Y_{2.93-x}Ln_xAl_5O_{12}:Ce_{0.07}$ (Ln = Gd, La) phosphors for white LEDs applicatio. *J. Alloy. Compd.* 498 (2010) 199–202.

[27] S. Uysal Satilmis, A. Ege, M. Ayvacikli, A. Khatab, E. Ekdal, E.J. Popovici, M. Henini, N. Can. Luminescence characterization of cerium doped yttrium gadolinium aluminate phosphors. *Opt. Mater.* 34 (2012) 1921–1925.

[28] Y.S. Zhao, J.S. Zhong, W.D. Xiang, W. Hua, H.L. Yang, J. Wang, W. Cai, Y.J. Dong, M.G. Shao. Mn-ion-enhanced red spectral emission from yttrium aluminum garnet doped cerium phosphor. *Chin. Sci. Bull.* 56 (2011) 3866–3870.

[29] N.S. Sawala, P.R. Somani, S.K. Omanwar. Near-infrared downconversion in Ce^{3+} – Yb^{3+} co-doped YAG. *J Mater Sci.* 28 (2017) 142–147.

[30] T. Ghrib, A.L. Al-Otaibi, M.A. Almessiere, A. Ashahri, I. Masoudi. Structural, optical and thermal properties of the Ce doped YAG synthesized by solid state reaction method. *Thermochim. Acta* 654 (2017) 35–39.

[31] A. Boukerika, L. Guerbous, M. Belamri. Effect of different annealing atmospheres on the structuraland luminescence properties of Ce^{3+}-doped YAG phosphors synthesized by sol – gel method. *Optik* 127 (2016) 5235–5239.

[32] A. Katelnikovas, P. Vitta, P. Pobedinskas, G. Tamulaitis, A. Zukauskas, J.-E. Jørgensenc, A. Kareiva. Photoluminescence in sol –gel-derived YAG:Ce phosphors. *J. Cryst. Growth* 304 (2007) 361 –368.

[33] H. Sun, X. Zhang, Z. Bai. Synthesis and characterization of nano-sized YAG:Ce,Sm spherical phosphors. *J. Rare Earth.* 31 (2013) 231–234

[34] J.Y. Park, H.C. Jung, G.S.R. Raju, J.H. Jeong, B.K. Moon, J.H. Kim, Y.K. Lee. Solvothermal synthesis and luminescence properties of the novel aluminum garnet phosphors for WLED applications. *Curr. Appl. Phys.* 13 (2013) 441–447.

[35] A. Aboulaich, J. Deschamps, R. Deloncle, A. Potdevin, B..Devouard, G. Chadeyron, R. Mahiou. Rapid synthesis of Ce^{3+}-doped YAG nanoparticles by a solvothermal method using metal carbonates as precursors. *New J. Chem*. 36 (2012) 2493 – 2500.

[36] L. Wang, F. Zhao, J. Zhuang, C. Pan, H. Huang. A facile route to Ce^{3+}-doped $Y_3Al_5O_{12}$ phosphors and their photoluminescent properties. *Mater. Lett.* 120 (2014) 163–165.

[37] G. Dantelle, M. Salaün, R. Bruyère, S. Kodjikian, A. Ibanez. Luminescent coatings prepared from optimized YAG:Ce nanoparticles. *Thin Solid Films* (2017) 10.1016/j.tsf.2017.05.001

[38] X. Li, H. Liu, J. Wang, H.i Cui, F. Han. YAG:Ce nano-sized phosphor particles prepared by a solvothermal method. *Mater. Res. Bull*. 39 (2004) 1923–1930.

[39] R. Guo, R. Zeng, Y. Wu, T. Wang, Y. Huang. preparation and photoluminescence properties of yag:ce^{3+} spherical phosphor nano-powders by the microemulsion method. *J. Chin. Ceram. Soc.* 36 (2008) 352–357.

[40] S. Mukherjee, V. Sudarsan, R.K. Vatsa, A.K. Tyagi. Luminescence studies on lanthanide ions (Eu^{3+}, Dy^{3+} and Tb^{3+}) doped YAG:Ce nano-phosphors. *J. Lumin.* 129 (2009) 69–72.

[41] S.R. Naik, T. Shripathi, A.V. Salker. Preparation, characterization and photoluminescent studies of Cr and Nd co-doped Ce:YAG compounds. *J. Lumin.* 161 (2015) 335–342.

[42] K.Y. Jung, Y.C. Kang. Luminescence comparison of YAG:Ce phosphors prepared by microwave heating and precipitation methods. *Physica B* 405 (2010) 1615–1618.

[43] A. Djebli, F. Boudjada, K. Pauwels, V. Kononets, G. Patton, A. Benaglia, M. Lucchini, F. Moretti, O. Sidletskiy, C. Dujardin, P. Lecoq, E. Auffray, K. Lebbou. Growth and characterization of Ce-doped YAG and LuAG fibers. *Opt. Mater.* 65 (2017) 66–68.

[44] H. Yamaguchi, K. Kamada, J. Pejchal, S. Kurosawa, Y. Shoji, Y. Yokota, Y. Ohashi, A. Yoshikawa. Effects of Mg-codoping on luminescence and scintillation properties of Ce doped $Lu_3(Ga,Al)_5O_{12}$ single crystals. *Opt. Mater.* 65 (2017) 60–65.

[45] F. Bi, G. Gai, X. Dong, S. Xiao, J. Wang, G. Liu, L. Zhao, L. Wang. Electrospinning preparation and photoluminescence properties of $Y_3Al_5O_{12}:Ce^{3+}$, Tb^{3+} nanobelts. *J. Mater. Sci.* 28 (2017) 4498 – 4505.

[46] W. Xiang, J. Zhong, Y. Zhao, B. Zhao, X. Liang, Y. Dong, Z. Zhang, Z. Chen, B. Liu. Growth and characterization of air annealing Mn-doped YAG:Ce single crystal for LED. *J. Alloy. Compd.* 542 (2012) 218–221.

[47] M. Li, D. Zhou, C.P. Li, Z. Zhao. Low temperature molten salt synthesis of YAG:Ce spherical powder and its thermally stable luminescent properties after post-annealing treatment. *Mat. Sci. Semicon. Proc.* 44 (2016) 101–107.

[48] L. Devys, G. Dantelle, G. Laurita, E. Homeyer, I. Gautier-Luneau, C. Dujardin, R. Seshadri, T. Gacoin. A strategy to increase phosphor brightness: Application with Ce^{3+}-doped $Gd_3Sc_2Al3O_{12}$. *J. Lumin.* 190 (2017) 62–68.

[49] W.T. Hong, J.H. Lee, J.W. Son, Z. Lee, H.J. Park, H.S. Kim, J.S. Lee, H.K. Yang. Color rendering improvement of the YAG:Ce^{3+} phosphors by co-doping with Gd^{3+} ions. *Ceram. Int.* 42 (2016) 2204–2208.

[50] G. Pari, A. Mookerjeee, A.K. Bhattacharya. Study of a-Al_2O_3 and the role of Y in $YAlO_3$ and $Y_3Al_5O_{12}$ by first principles electronic structure calculations. *Physica B* 353 (2004) 192–200.

[51] L. Grigorjeva, D. Jankoviča, K. Smits, D. Millers, S. Zazubovich. Defect luminescence of YAG nanopowders and crystals. *Latvian J. Phys. Techn. Sci*. 4 (2012) 54–60.

[52] A. Vedda, D. Di Martino, M. Martina, J. Mares, E. Mihokova, M.

Nikl, N. Solovieva, K. Blazek, K. Nejezchleb. Trap levels in Y-aluminum garnet scintillating crystals. *Radiat. Meas.* 38 (2004) 673–676.

[53] C.R. Stanek, K.J. McClellan, M.R. Levy, R.W. Grimes. Extrinsic defect structure of $RE_3Al_5O_{12}$ garnets. *Phys. Status Solidi B* 243 (2006) R75–R77.

[54] J.W.H. Van Krevel, H.T. Hintzen, R. Metselaar, A. Meijerink. Long wavelength Ce^{3+} emission in Y-Si-O-N materials. *J. Alloys Compd.* 268 (1998) 272–277.

[55] Y.Q. Li, J.E.J. van Steen, J.W.H. van Krevel, G. Botty, A.C.A. Delsing, F.J. DiSalvo, G. de With, H.T. Hintzen. *J. Alloys Compd.* 417 (2006) 273–279.

[56] S.P. Lee, T.S. Chan, T.M. Chen. A novel reddish orange-emitting $BaLa_2Si_2S_8:Eu^{2+}$ Thiosilicate Phosphor for LED Lighting. *ACS Appl. Mat. Interf.* 7 (2015) 40–44.

[57] V. Bachmann, C.R. Ronda, O. Oeckler, W. Schnick, A. Meijerink. Color point tuning for $(Sr,Ca,Ba)Si_2O_2N_2:Eu^{2+}$ for white light LEDs. *Chem. Mater.* 21 (2009) 316–325.

[58] B.G. Zhai, L. Yang, Q.L. Ma, Y.M. Huang. First-principles calculations of band structures and optical properties of hexagonal ZnO by using meta-GGA in the framework of density functional theory. *Optoelectron. Mater*. 1 (2016) 13–17.

[59] B.G. Zhai, C. Tang, Y.M. Huang. First-principles density functional calculations of the band structures of $SrAl_2O_4$. *Optoelectron. Mater*. 1 (2016) 18–21.

[60] B.G. Zhai, L. Yang, J.S. Li, Y.M. Huang. Density functional calculations on the electronic structures of triclinic $ZnMoO_4$. *Optoelectron. Mater.* 1 (2016) 43–49.